JOURNAL OF PROPULSION AND POWER
Vol. 10, No. 6, Nov.–Dec. 1994

Numerical Solutions of Two-Dimensional Multistage Rotor/Stator Unsteady Flow Interactions

R.-J. Yang* and S.-J. Lin†
Rockwell International, Canoga Park, California 91303

A two-dimensional, Navier-Stokes, multizone approach has been used to investigate unsteady flow interactions within two multistage axial turbines. The governing equations are solved by an iterative, factored, implicit finite difference, upwind algorithm. For the numerical accuracy check, investigations are also carried out on the effect of temporal accuracy, the effect of subiteration in the Newton-Raphson technique, and the effect of full viscous vs thin-layer calculation. Computed results of a one and one-half-stage calculation compare well with experimental data. Unsteady flow interactions, wake cutting, and the associated evolution of vortical entities are discussed. Computed results of a six-stage calculation also compare well with engine balanced data obtained from a classical one-dimensional analysis. The calculated transient accurate solutions provide much information for component analysis, especially for computing the forcing function used in a structural dynamic analysis.

Introduction

MOST turbomachines consist of rotating components. In the case of a turbine configuration, a row of stationary vanes (stator) is followed by a rotating wheel of blades (rotor). The vanes accelerate and direct the flow that impacts the blades and drives the turbine. Whenever the blades pass through the wakes generated by the trailing edges of the vanes (i.e., wake cutting), unsteady loading on the blades results. Besides the wake cutting effects, the flow is inherently unsteady because of potential effects between the stationary and rotating airfoils and vortex shedding by blunt trailing edges of the airfoils. The interaction effects are known to affect many aspects of turbomachinery performance including blade loading, stage efficiency, heat transfer, stall margin, and noise generation. In particular, accurate estimation of dynamic loading is important to designers. The cyclic dynamic loading may cause high-cycle fatigue to the airfoils. If the frequency of the loading corresponds with the natural frequency of the system, the resonant effect may result in structure failure. Therefore, an accurate transient solution of the rotor-stator flow would be very useful.

Rai[1] presented a one-stator/one-rotor interaction study. His calculation was performed on a system of patched and overlaid grids using the unsteady, thin-layer, Navier-Stokes equations in two dimensions. The airfoil geometries and flow conditions were the same as those in Ref. 2. Good agreement between the calculation and the experimental result of Ref. 2 was obtained in the case of time-averaged surface pressures on the stator and rotor. Unsteady pressure amplitudes were also in reasonable agreement. Rai[3] extended his method to a multistator/multirotor calculation with a closer approximation to the experimental airfoil geometries. It was found that the time-averaged pressures were nearly identical to those of the one-stator/one-rotor case. However, a significant improvement in unsteady pressure amplitude and phase were obtained. Yang et al.[4] applied the method of Rai[1] to calculate the unsteady aerodynamics of a one-stator/one-rotor configuration in the high-pressure oxidizer turbopump (HPOTP) of the Space Shuttle main engine (SSME). They described the vortex shedding and wake cutting process and the associated unsteady convection of large-scale vortical motion. They also found that a small time-step size was required to resolve unsteady components in the flowfield. Lin and Yang[5] applied the method of Rai[3] to simulate the multistator/multirotor configuration in the SSME high-pressure fuel turbopump (HPFTP). They performed spatial and temporal accuracy studies to determine maximum time-step and grid sizes within engineering accuracy and with minimum computational costs. The study showed that a factor of 10 reduction in computer time could be achieved by judiciously enlarging time-step size and reducing the total number of grid points for the configurations considered. Griffin and McConnaughey[6] applied Rai's method[1] to compute unsteady heat transfer coefficients for stator/rotor configurations. Their computed results compared well with experimental data.

The studies reported previously are for single-stage configurations. It is useful to extend Rai's method to multistage configurations because most turbomachines have multistage rotating components. This is particularly true if one is interested in those parts after the first stage. The reason is that wake effects are important for characterization of unsteady flow features in the downstream stages. If one uses a single-stage approach, a time-dependent wake condition at the inlet must be specified. Usually the wake condition is not known except as provided by experiments. For a general approach, using a multistage method, the wake information is directly obtained from numerical solutions.

Gundy-Burlet et al.[7,8] presented an extension of the Rai's method[1,3] that incorporates multistage capability. A two and one-half-stage compressor flow was analyzed. Their computed results compared well with experimental data. In this study, we independently extend the Rai's method[1,3] to compute multistage turbine flows. To validate the method, a calculation using the United Technology Research Center (UTRC) one and one-half-stage large-scale rotating rig (LSRR) case is performed. Computed results in the form of time-averaged static pressure and unsteady pressure amplitude on airfoil surfaces are presented and compared with experimental data. Numerical accuracy is investigated by a series of parameter studies. The studies include the effect of time-step size, the effect of subiteration in the Newton-Raphson technique, and the effect of full viscous vs thin-layer approximation. Finally, an application of the method to a six-stage axial turbine in the SSME low-pressure oxidizer turbopump (LPOTP) is demonstrated. Comparisons are made between the multistage

Received May 31, 1991; revision received July 20, 1993; accepted for publication April 7, 1994.

*Senior Member of Technical Staff, Rocketdyne Division; currently at the Department of Engineering Science, National Cheng Kung University, Tainan, Taiwan, Republic of China. Member AIAA.

†Senior Member of Technical Staff, Rocketdyne Division. Member AIAA.

calculation and a classical one-dimensional analysis. Applications of the method to other multistage rotor/stator configurations can be found in Lin and Yang.[9]

Technical Approach

Rai's method[1,3] for a single-stage case is adopted as a basis for the present study. A multizone grid system is used. For each airfoil there are two grid zones, namely, one inner "O" grid and one outer "H" grid. The inner O grid encloses the airfoil surface and accurately resolves the leading and trailing edges. The O grid is generated using an elliptic grid generator with the condition that the grid be orthogonal to the airfoil surface. The H grid is generated algebraically with the requirement that the metric coefficients be continuous across the periodic lines where periodic boundary conditions are imposed. A region of overlap exists between the O and H grids. The vane and blade grid systems are separated by a common patch boundary to facilitate movements of the rotor grid system without any distortion of the grid lines. Information transfer between the different zones is affected by proper imposition of interface boundary conditions.

The unsteady, thin-layer Navier-Stokes equations in the O grid zones, and the unsteady Euler equations in the H grid zones are solved. The governing equations are cast in the strong conservation form. The numerical procedure used to solve the governing equations is an iterative, factored, implicit scheme. The procedure is discussed in detail in Ref. 1. The method can be outlined as follows. The governing equations are replaced by a fully implicit finite-difference approximation. Numerical fluxes are evaluated by the third-order accurate upwind-biased Osher scheme.[10] The resulting system of nonlinear equations is solved by the Newton-Raphson iteration technique. To solve these difference equations at each iteration level, an approximate factorization method is used. This technique leads to a system of coupled linear difference equations with narrow block-banded structures that can be solved efficiently by a LU decomposition method. Some subiterations may be used at each time-step to reduce linearization and factorization errors.

During the interaction process, rotor airfoils move relative to stator airfoils. An accurate method for information transfer between stationary and moving grids is necessary for multistage interaction problems. Rai[1] has developed an accurate method for single-stage problems. Its extension to the multistage case is straightforward. Note that for a single-stage case, there is only one moving patched boundary. For an n-stage case, there are $2n - 1$ moving patched boundaries.

The use of multiple zones in simulating flows over rotor/stator configurations results in several computational boundaries, namely, inlet, exit, solid surface, periodic, and zonal (overlap and patch) boundaries. The boundary conditions used at each of these boundaries are addressed in detail in Refs. 1 and 3, and thus are omitted here.

Flows associated with rotor/stator configurations are unsteady in nature due to periodic interaction effects. In addition, the flow might have transition from laminar to turbulence along airfoil surfaces. Near the trailing edges of airfoils, there exist large-scale wake structures. Conventional turbulence models are developed to calculate steady mean flows. For unsteady turbulent flows, advanced turbulence models are required. As a starting point for the rotor/stator flow calculations, the Baldwin-Lomax model[11] is used in the current studies. The kinematic viscosity is evaluated using Sutherland's law.

Computed Results and Discussion

Two cases with different rotor/stator configurations and flow conditions are calculated by integrating the equations of motion and the boundary conditions described earlier. Case 1 is the UTRC one and one-half-stage LSRR. Case 2 is the six-stage axial turbine in the SSME LPOTP.

Case 1: UTRC One and One-Half-Stage LSRR

Figure 1 shows the configuration of case 1. There are 22:28:28 airfoils in each blade row, respectively. In the computation we use 21:28:28 airfoils, with a common factor of 7, so that only 3:4:4 airfoils are computed and periodic boundary conditions are used to simulate the effects of other airfoils. To keep blockage effects the same, the first-stage stator airfoil geometry is enlarged by a factor of 22/21, keeping the pitch-to-chord ratio constant. Note that the first-stage rotor and second-stage stator airfoil geometries are the same as the experiment in Ref. 12. The inner O grid zone for each airfoil contains 101 × 21 points. For the outer H grid zone, the first-stage stator airfoil contains 65 × 31 points, the rotor airfoil contains 65 × 31 points, and the second-stage stator airfoil contains 88 × 31 points, respectively. The total grid points for the entire 11 airfoils are 48,348. The minimum mesh size is 0.0001 in. normal to the airfoil surfaces. Figure 2 shows the grid system (for the sake of clarity not every grid line is plotted). The flow conditions are an inlet Mach number of 0.07, a Reynolds number of 4.0×10^4/in. (this Reynolds number is very close to the experimental value used in Refs. 2 and 12 and is lower than the value used by Rai[1,3]), and a flow coefficient of 0.78 (ratio of inlet flow velocity to rotor velocity). Because the quantities prescribed at the inlet boundary are the Riemann invariants and not the dependent variables themselves, the values of u, v, p, and ρ obtained at the inlet, when the solution becomes periodic in time, are generally different from those used to determine the Riemann invariants. To match the inlet flow condition, the ratio of the exit static pressure to the inlet total pressure needs to be

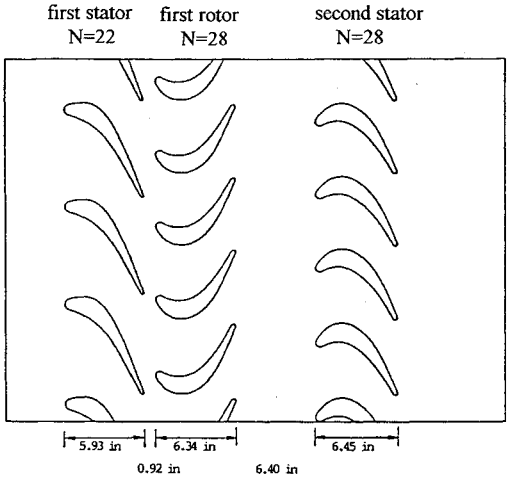

Fig. 1 UTRC 1.5-stage LSRR.

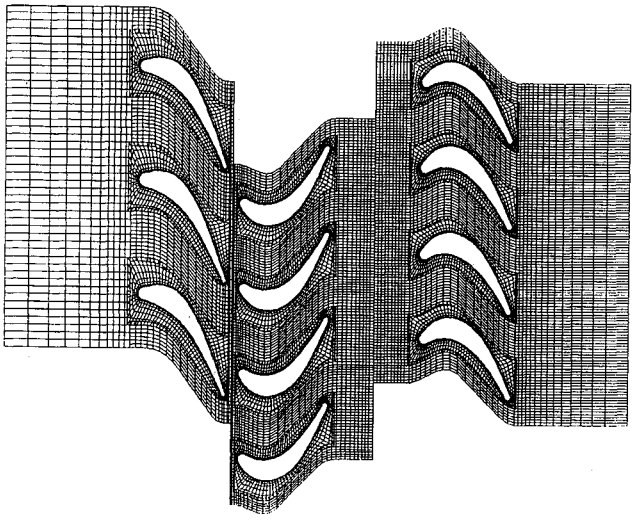

Fig. 2 Multizone grid system.

adjusted and the calculations need to be continued until the calculated flow coefficient is equal to the specified value. In the present calculation, the final pressure ratio is 0.95.

Figure 3 shows the time-averaged pressure coefficient C_p and the unsteady pressure envelope on the airfoil surfaces. The pressure coefficient is defined as

$$C_p = \frac{P_{\text{avg}} - P_{t\,\text{inlet}}}{\frac{1}{2}\rho_{\text{inlet}}\omega^2}$$

where P_{avg} is the static pressure averaged over one composite cycle, $P_{t\,\text{inlet}}$ is the averaged total pressure at the inlet, ρ_{inlet} is the averaged density at the inlet, and ω is the velocity of the rotor airfoils. The shaded area represents the range of the fluctuating pressure in a composite cycle. A composite cycle corresponds to the motion of the rotor through an angle equal to $6\pi/21$, where 21 is the number of first-stage stator airfoils. Clearly, there is good agreement between the prediction and experimental data. There is no experimental data available for the second-stage stator. The figure indicates that the unsteadiness is appreciable only on the first-stage stator airfoil suction side near its trailing edge. On the other hand, the flow is seen to be unsteady over the entire first-stage rotor and second-stage stator surfaces. The fluctuating pressure on the first-stage stator is due to the upstream potential interaction between the downstream airfoils and the first-stage stator airfoil, whereas that on the first-stage rotor and the second-stage stator is due to the combined influence of potential interaction, wake/airfoil, and wake/wake interactions.

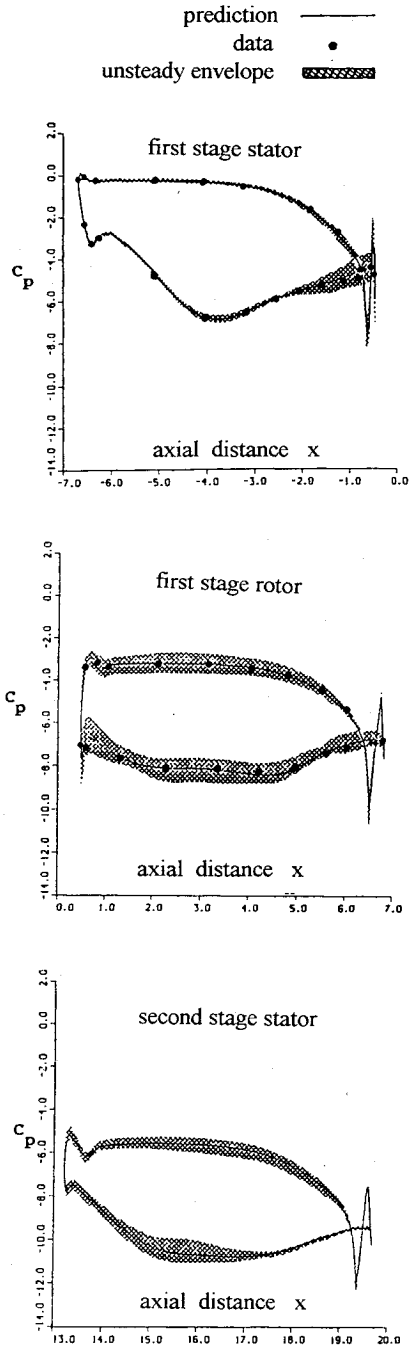

Fig. 3 Time-averaged pressure coefficient and unsteady pressure envelope on airfoil surfaces.

It has been shown that the predicted time-averaged pressure coefficients agree quite well with the experimental data. Generally speaking, the first-order mean flow quantities are easier to compute than the second-order fluctuating flow quantities. Our experience indicated that small time-step size was required to resolve fluctuating quantities. As numerical accuracy checks, we perform the following investigations: the effect of full viscous vs thin-layer approximation, the effect of time-step size, and the effect of subiteration. These investigations show that mean flow quantities are nearly unaffected by these factors. Therefore, only fluctuating pressure amplitudes are presented.

Full Viscous vs Thin-Layer Approximation

For most engineering flow calculations, grid meshes are placed parallel to the streamwise direction (e.g., the ξ direction). It is generally believed that the streamwise viscous effect cannot be resolved unless fine grid mesh is used. Therefore, thin-layer approximation (i.e., neglect of streamwise viscous term) is used in the flow calculations. For the current geometry, an O grid mesh is used to wrap around airfoil surfaces. The primary flow direction near leading and trailing edges of the airfoils is not parallel to body surfaces. The primary flow direction changes from the ξ direction to the η direction, especially near trailing edges, and thus the ξ direction has a dominant viscous effect and should not be neglected. Furthermore, flow separation may exist at the airfoil trailing edges. Therefore, the effect of a full viscous calculation is investigated. When solving the Navier-Stokes equations, for simplicity, the ξ direction viscous term is implemented explicitly in the code. This treatment should not affect the numerical accuracy since the subiteration in the Newton-Raphson technique is employed.

Figure 4 shows the fluctuating pressure amplitude coefficients for both full viscous and thin-layer computations (3000 time-steps per composite cycle and 3 subiterations are used in the calculations) and comparisons with the experimental data. The magnitude of temporal pressure fluctuating C_p is defined as

$$C_p = \frac{P_{\max} - P_{\min}}{\frac{1}{2}\rho_{\text{inlet}}\omega^2}$$

where $P_{\max}$ and $P_{\min}$ are the maximum and minimum pressure occurring over a composite cycle at a given point. Full viscous and thin-layer computations both agree well with the experimental data. There is no experimental data available for the second-stage stator. It demonstrates that the viscous effect on unsteady pressure fluctuation near trailing edges of the airfoils is small when compared with the inviscid mechanism. It is known that the shear layer type of wake is unstable. It is an inviscid instability so that the shear layers would roll up into discrete vortical entities. The pressure fluctuation associated with the evolution of the inviscid vortical entities tends to be larger than that associated with viscous effects.

Effect of Time-Step Size

Time resolution of temporal flow structures is one of the major factors in determining numerical accuracy for unsteady flow problems. Time scales associated with the rotor/stator

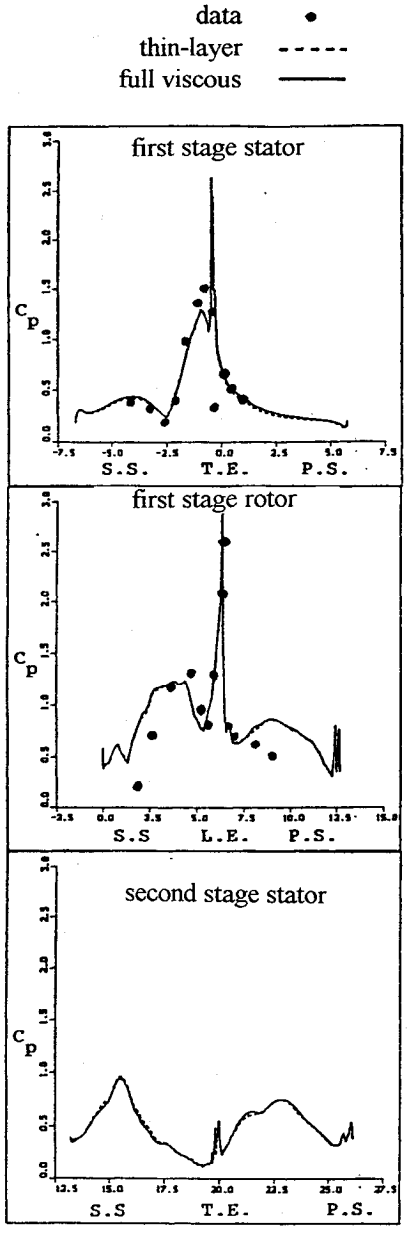

Fig. 4 Effect of full viscous vs thin-layer calculation on the fluctuating pressure amplitude.

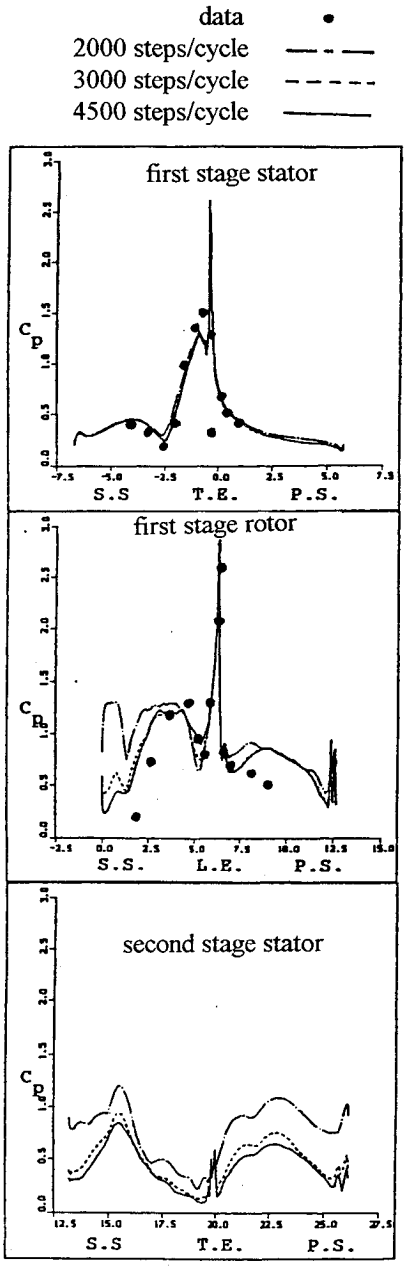

Fig. 5 Effect of time-step size on the fluctuating pressure amplitude.

unsteady flow interaction arise from rotor rotation, vortex shedding, wake convection, and acoustic scales. These scales may range from very large to very small, depending on geometry and flow conditions. We perform the following calculations using 2000, 3000, and 4500 time-steps, respectively, in a composite cycle. Three subiterations are used in each calculation. Figure 5 shows the computed results and comparisons with the experimental data. The result indicates the following: 1) as the time-step size becomes smaller, the solutions coincide with one another asymptotically, and 2) upstream potential effect on the first-stage stator fluctuating pressure is well resolved within the time-step sizes considered. Some improvements are also observed in the periodic behavior of the pressure with increasing number of time-steps per cycle. The reason for this may be either 1) the pressure perturbations due to vortex shedding are smaller than the differences in pressure from cycle to cycle, or 2) the shedding frequency has somehow locked onto the blade passing frequency.

Effect of Subiteration

The nonlinear Navier-Stokes equations are solved by the Newton-Raphson iteration technique in the present method. Linearization and factorization errors can be driven to zero at each time-step if a solution can be converged by the Newton-Raphson iteration. It is known that using the compressible flow formulation to simulate low Mach number flows may result in large factorization error within the framework of the alternating direction implicit (ADI) method. We perform the calculations to investigate the combined effects of linearization and factorization errors on the fluctuating pressure amplitude. We use 4500 time-steps in a composite cycle; 1, 2, and 3 subiterations are employed, respectively. Since temporal truncation errors are the same in these cases, any differences in the solutions are due to linearization and factorization errors. Figure 6 shows the computed results and comparisons with the experimental data. Solutions using both 2 and 3 subiterations are nearly identical to each other. Only small deviations from the experimental data are observed in results with 1 subiteration. Comparing Figs. 5 and 6 (see the case of 4500 steps/cycle with 2 subiterations and 3000 steps/cycle with 3 subiterations, these two cases have the same computing costs), it is felt that the effect of time-step size is more effective in reducing the errors. Heuristically, small time-step size reduces linearization, factorization, and temporal

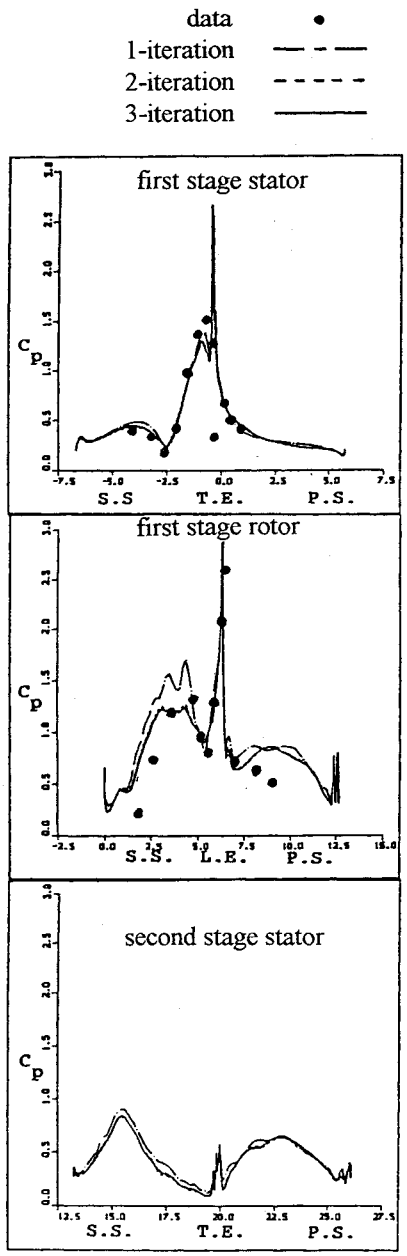

Fig. 6 Effect of subiteration on the fluctuating pressure amplitude.

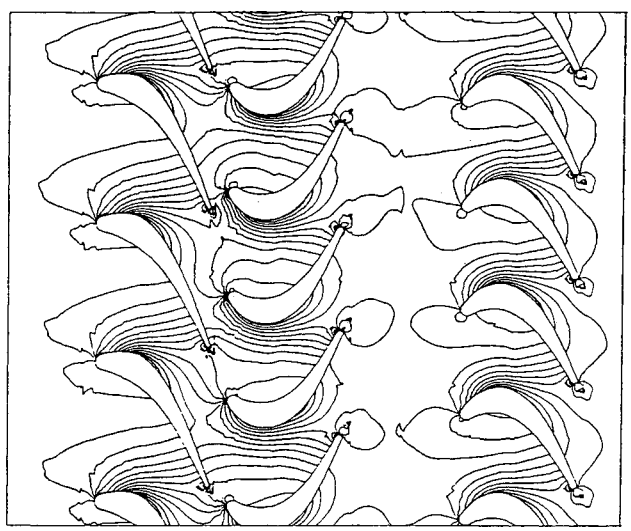

Fig. 7 UTRC LSRR instantaneous pressure contours.

truncation errors. Then we ask: is subiteration necessary if a smaller time-step size is used? We perform the calculations using 6000 steps/cycle with 1 subiteration. The computed results turn out to be nearly identical to that of 4500 steps/cycle with 1 subiteration. Thus, subiteration is still necessary to reduce linearization and factorization errors for the flow considered here.

Figures 7 and 8 show the pressure and Mach number contours at one instant. At first-stage stator passages, flow features are almost unchanged except near its trailing edges. Different flow features are observed at the first-stage rotor and second-stage stator passages. The differences are due to wake effects. Wakes are generated by the trailing edges of the stator and rotor airfoils. The wakes roll up into vortical entities. These entities are embedded in and convected by the mean flow. Because of the rotor rotation, the wakes generated by the first-stage stator are chopped and sheared (rotor suction side has higher velocity than pressure side) and convected along the rotor passages. They interact with the rotor airfoils and other wakes generated by the rotor trailing edges. The combined wakes are convected into second-stage passages and more complex interaction takes place. Figure 9 (unsteady vectors) and Fig. 10 (entropy contours) illustrate the phenomena described previously. Unsteady vectors are obtained by subtracting the mean flow vectors from the instantaneous

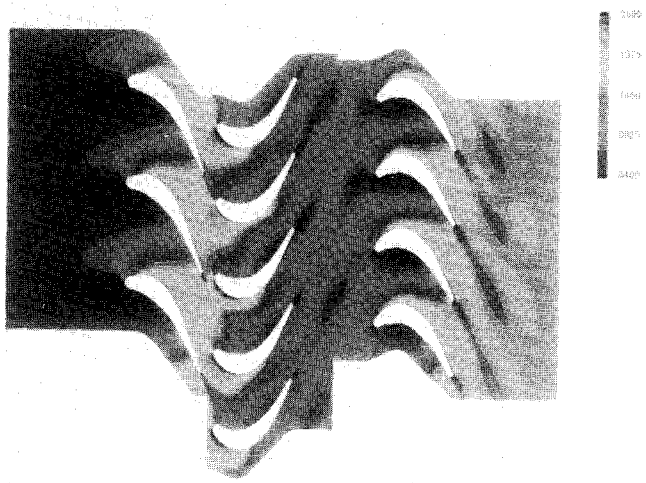

Fig. 8 UTRC LSRR instantaneous Mach number contours.

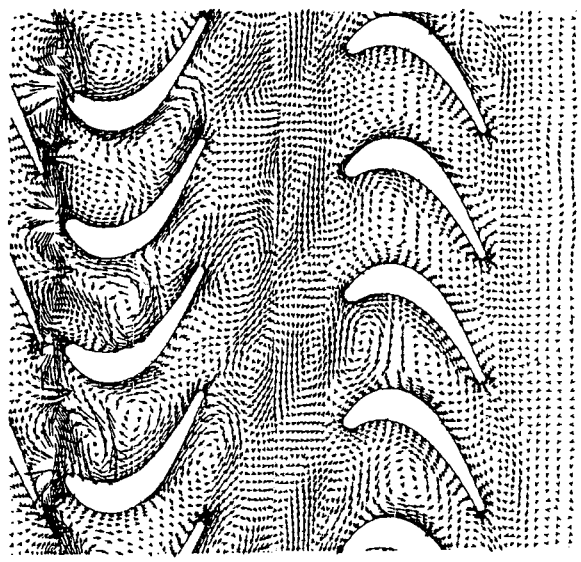

Fig. 9 UTRC LSRR unsteady velocity vectors.

flow vectors. They clearly reveal large-scale structures of vortical entities.

Entropy is a signature of fluid loss due to boundary layer and wake effects for the current rotor/stator flow. Figure 10 shows entropy contours at one instant. It reveals that wakes remain coherent downstream. It clearly shows that the loss is confined to the airfoil surfaces for the first-stage stator. The wakes are shed from the first-stage airfoil trailing edges. At different relative locations, the wakes are chopped and distorted by the rotor as indicated by the notations 1, 2, and 3. Along the rotor passage, high-loss fluid is convected toward the suction side, and low-loss fluid is transported toward the pressure side to replace the migrated wake fluid (see Figs. 9 and 10). The high-loss fluid mixes with rotor wakes as shown by the notations 4, 5, and 6 in Fig. 10. The entropy contours show some pulsations along the paths of the wakes (see notations from 4 to 9). The combined high-loss fluids from first-stage airfoils (stator and rotor) are convected coherently into the second-stage stator passage. These high-loss fluids are distorted by the second-stage airfoils. Many complicated interactions, e.g., wake/wake and wake/airfoil interactions, occur in the second stage.

The contours in Figs. 7, 8, and 10 show small wiggles across zonal boundaries. The reason is mainly due to the mismatched grids on either side of the zonal boundaries that may have large differences in mesh sizes. Therefore, the first-order interpolation (linear weighting) for flow variables between zones may not accurately represent the true physics.

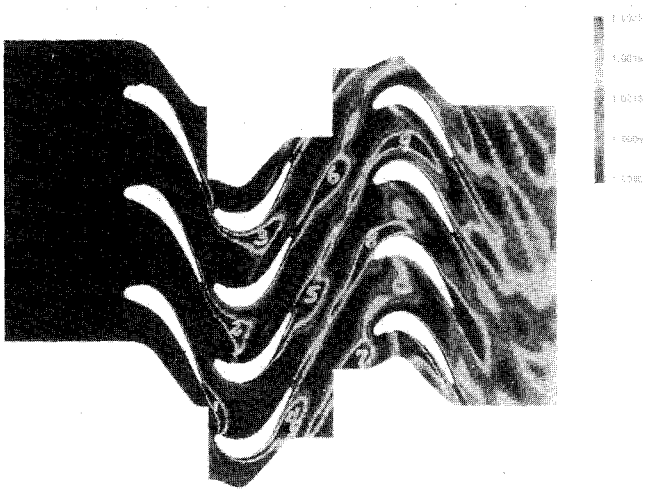

Fig. 10 UTRC LSRR instantaneous entropy contours.

Case 2: SSME Six-Stage LPOTP

There are 43 and 67 airfoils in the first-stage stator and rotor, respectively. From second to sixth stage, they have identical configurations with 61 and 67 airfoils in the stator and rotor, respectively. For the sake of computational economy, only 12 airfoils are chosen in the calculation, i.e., the ratio of the stator airfoil to rotor airfoil is 1:1 from the first to the sixth stage. In so doing, and keeping blockage effects the same, the first-stage stator airfoil is scaled by a factor of 43/67, and those stator airfoils after the first stage are scaled by a factor of 61/67, keeping the pitch-to-chord ratio constant. The geometries of rotor airfoils in the entire six stages are unchanged. The flow conditions are an inlet Mach number of 0.05, a Reynolds number of 2.5×10^6/in., and a flow coefficient of 0.396. We use 500 steps per cycle with one subiteration to eliminate transient disturbances. During the transient calculation, the exit static pressure is gradually adjusted to establish the specified flow coefficient. It takes about 30 cycles (around 8 h of CPU time on a Cray Y-MP machine) to reach the flow condition. Since there is no experimental data available for this case, for a conservative calculation, we continue the computation using 2000 steps/cycle with 3 subiterations. It takes another 5 cycles to achieve a time-periodic solution.

Figure 11 shows the C_p and unsteady pressure envelope on the stator and rotor airfoils for the fourth-stage turbine. The other C_p profiles for the rest of the stages have similar shapes except a nearly constant value difference. However, the stator and rotor C_p profiles are getting blunter near the leading edges of the airfoils along the downstream stages. This indicates the flow incidence angle to the airfoil is different from stage to stage, albeit the stage geometries are identical to each other (except the first stator). If we assume the flow is incompressible and inviscid, it can be shown that the relative inflow angles to both stator and rotor airfoils remain the same from the second to the sixth stage. The static pressure drop across each stage can also be shown to be constant. In the current solutions, the inflow angles and the static pressure drops are given in Table 1 along with the engine balanced data. The engine balanced data are obtained from a one-dimensional, inviscid, quasisteady analysis corrected with viscous and tip clearance effects in Ref. 13. The stator inflow angles are increasing along the downstream stages. The reason for this increase in angles is mainly due to compressible effect. Recall the inlet Mach number is 0.05, which is practically incompressible. In the multistage computation, the highest Mach number in the flowfield is about 0.35, yielding variations in density. For the conservation of mass, the axial velocity component gradually increases along the downstream stages. This is in contrast to the incompressible analysis in which the axial velocity component is constant.

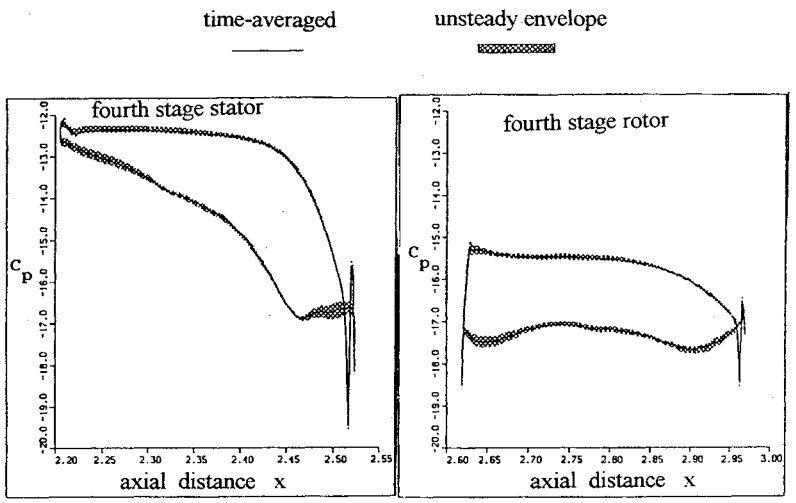

Fig. 11 SSME LPOTP time-averaged pressure coefficient and unsteady pressure envelope on the fourth stage stator and rotor surfaces.

Table 1 Inflow angles to stator airfoils and static pressure drop across each stage

Stage no.	Multistage solution	One-dimensional analysis	Incompressible
	a) Stator inflow angles, deg		
1	0	0	0
2	18.9	16.6	14.8
3	22.2	21.7	14.8
4	27.4	26.8	14.8
5	31.9	31.7	14.8
6	36.7	36.4	14.8
	b) Static pressure drop across each stage, psi		
1	537	635	618
2	621	648	618
3	648	669	618
4	675	695	618
5	698	726	618
6	731	764	618

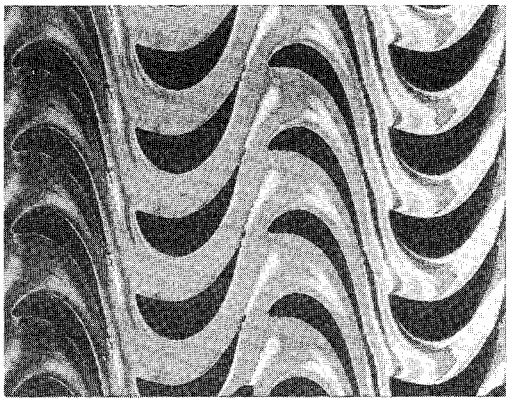

Fig. 12 Instantaneous entropy contours for the LPOTP fourth and fifth stages.

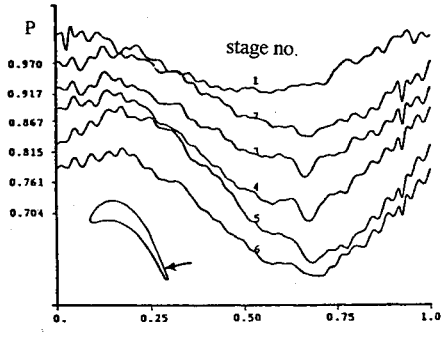

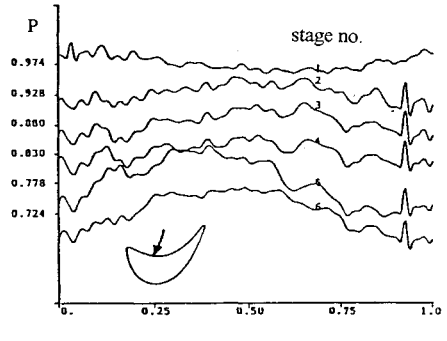

Fig. 13 Pressure history on a) stator surface and b) on rotor surface.

The upstream wakes are convected and interacted with the downstream wakes and airfoils. The accumulation of the wakes at the downstream stages generates complex flow structures. Figure 12 shows instantaneous entropy contours for the fourth and fifth stages. It depicts different instantaneous flow features from stage to stage. The flow within the downstream stages is more complicated than the upstream stages, indicating the importance of using multistage computation to obtain accurate flow information. The time variation of the static pressure at an identical location in both stator and rotor airfoil surfaces is shown in Fig. 13. The major shape is similar, but local variations do exist. The amplitude is getting bigger along downstream stages. It is believed that the major contribution to the unsteadiness is from the adjacent wake effects. Further upstream, wakes are a minor contribution because of physical and numerical dissipation. It clearly shows time variations of the pressure history.

The classical design method does not consider unsteady effects. The unsteady effects may be important in the issue of material stress fatigue and structure resonance problems. To demonstrate the application of the current calculation, a structural dynamic analysis is illustrated. The computed unsteady pressure distributions were applied to calculate instantaneous generalized force for structural dynamic analysis in Ref. 14. The results of this analysis indicated no high-cycle fatigue problems. The unsteady pressure history can also be decomposed into various harmonics and amplitudes by the Fourier series analysis. Note that the amplitudes of the unsteady pressure may be small, yet their frequencies may coincide with the natural frequency of the structure and result in resonance. Detailed discussion of this application is beyond the scope of this article. The present multistage calculation provides much information that is useful for the component analysis.

Summary

Two different axial multistage turbines are simulated: 1) the one and one-half-stage of the UTRC LSRR and 2) the six-stage SSME LPOTP. Numerical accuracy for the UTRC case is checked by investigating the effect of full viscous vs thin-layer approximation, the effect of time-step size, and the effect of subiteration in the Newton-Raphson technique. The shear layer type of wake near the trailing edge of every airfoil rolls up into large-scale vortical entities. It is an inviscid mechanism associated with the evolution of the vortical entities. The unsteady pressure fluctuation produced by the inviscid mechanism is larger than that of viscous effect. Small time-step size is effective in reducing errors caused by linearization, factorization, and truncation, however, subiteration is still necessary to reduce linearization and factorization errors for the flow considered.

Wakes are convected coherently into downstream stages. Interactions between wake/airfoil and wake/wake are common. For the case of six-stage SSME LPOTP, although they have identical stage geometries along downstream, the stator inflow angles to the airfoils are different from stage to stage. The different inflow angles result in different pressure loading near the leading edges of the airfoils. The present multistage and transient accurate solutions provide unsteady pressure information for computing forcing functions used in structural dynamic analysis. This information can be used in the analysis of high-cycle fatigue and frequency resonant problems. The calculations demonstrate how the CFD can be used in the analysis of real-world engine problems.

Acknowledgments

This work was sponsored by NASA Marshall Space Flight Center (MSFC), Huntsville, Alabama. Computation resources were provided by NAS systems at NASA Ames Research Center, Moffett Field, California. The authors would like to express their appreciation for the support and en-

couragement given by M. M. Rai and his colleagues at NASA Ames, and H. V. McConnaughey at NASA MSFC. Color graphics were made by K. Sheedy at Rocketdyne, Conoga Park, California. Our appreciation is extended to C. L. Merkle of the Pennsylvania State University, University Park, Pennsylvania, for his comments on this work.

References

[1]Rai, M. M., "Navier-Stokes Simulations of Rotor-Stator Interactions Using Patched and Overlaid Grids," *Journal of Propulsion and Power*, Vol. 3, No. 5, 1987, pp. 387–396.

[2]Dring, R. P., Joslyn, H. D., Hardin, L. W., and Wagner, J. H., "Turbine Rotor-Stator Interaction," *Journal of Engineering for Power*, Vol. 104, Oct. 1982, pp. 729–742.

[3]Rai, M. M., and Madavan, N. K., "Multi-Airfoil Navier-Stokes Simulations of Turbine Rotor-Stator Interaction," *Journal of Turbomachinery*, Vol. 112, July 1990, pp. 377–384.

[4]Yang, R.-J., Lin, S.-J., and Rai, M. M., "Unsteady Aerodynamics of Rotor-Stator Interaction in a Turbine Stage," AIAA Paper 88-0360, Jan. 1988.

[5]Lin, S.-J., and Yang, R.-J., "Multi-Blade Navier-Stokes Simulations of Rotor-Stator Interaction in a Turbine Stage," AIAA Paper 89-0326, Jan. 1989.

[6]Griffin, L. W., and McConnaughey, H. V., "Prediction of the Aerodynamic Environment and Heat Transfer for Rotor/Stator Configurations," American Society of Mechanical Engineers Paper 89-GT-89, 1989.

[7]Gundy-Burlet, K. L., Rai, M. M., and Dring, R. P., "Two-Dimensional Computations of Multi-Stage Compressor Flows Using a Zonal Approach," AIAA Paper 89-2452, July 1989.

[8]Gundy-Burlet, K. L., Rai, M. M., Stauter, R. C., and Dring, R. P., "Temporally and Spatially Resolved Flow in a Two-Stage Axial Compressor: Part 2—Computational Assessment," *Journal of Turbomachinery*, Vol. 113, April 1991, pp. 227–232.

[9]Lin, S.-J., and Yang, R.-J., "Viscous Unsteady Computations of Rotor/Stator Flows in the Multi-Stage Turbines," AIAA Paper 91-2465, July 1991.

[10]Rai, M. M., and Chakravarthy, S. R., "An Implicit Form for the Osher Upwind Scheme," *AIAA Journal*, Vol. 24, No. 5, 1986, pp. 735–743.

[11]Baldwin, B. S., and Lomax, H., "Thin-Layer Approximation and Algebraic Model for Separated Turbulent Flows," AIAA Paper 78-257, Jan. 1978.

[12]Dring, R. P., Blair, M. F., Joslyn, H. D., Power, G. D., and Verdon, J. M., "The Effects of Inlet Turbulence and Rotor/Stator Interactions on the Aerodynamics and Heat Transfer of a Large-Scale Rotating Turbine Model," Final Rept., NASA CR-4079, 1986.

[13]Tran, K., private communication, Rocketdyne/Rockwell International, Canoga Park, CA, 1992.

[14]Gage, S. S., "LPOTP Stator Vane Structural Dynamic Analysis," Rocketdyne/Rockwell International Internal Rept., IL-90-133-30-21, Canoga Park, CA, Dec. 1990.